HHS Public Access

Author manuscript

Biorheology. Author manuscript; available in PMC 2016 September 12.

Published in final edited form as:

Biorheology. 2015 ; 52(5-6): 447–463. doi:10.3233/BIR-15067.

Atrial natriuretic peptide down-regulates neutrophil recruitment on inflamed endothelium by reducing cell deformability and resistance to detachment force

Vasilios A. Morikis[a], **Chris Radecke**[a], **Yanyan Jiang**[a], **Volkmar Heinrich**[a], **Fitz-Roy Curry**[a,b], and **Scott I. Simon**[a,*]

[a]Department of Biomedical Engineering, University of California, Davis, CA 95616, USA

[b]Department of Physiology and Membrane Biology, School of Medicine, University of California, Davis, CA 95616, USA

Abstract

BACKGROUND—Recombinant atrial natriuretic peptide (ANP) is administered in patients with acute heart failure in Japan to improve renal function and hemodynamics, but its anti-inflammatory effect on activated leukocytes may also contribute to its therapeutic efficacy.

OBJECTIVE—Examine unconventional role of ANP in neutrophil adhesion to inflamed endothelium.

METHODS—Human neutrophils were perfused over endothelial monolayers in a microfluidic lab-chip assay. Cell rheology was assessed by micropipette aspiration to assess changes in cortical tension and viscosity. Fluorescence microscopy was applied to measure adhesive contact area and β_2-integrin focal bond formation.

RESULTS—ANP inhibited neutrophil rolling and firm adhesion without influencing the upregulation of cellular adhesion molecules on endothelium or the regulation of high affinity CD18 and shedding of L-selectin during neutrophil activation. Exposed to fluid shear, integrin mediated arrest was disrupted with ANP treatment, which elicited formation of long tethers and diminished cell spreading and contact. This correlated with a ~40% increase in neutrophil viscosity and a reduction in the adhesive footprint.

CONCLUSIONS—A decrease in cell deformation and neutrophil flattening with ANP results in fewer integrin bond clusters, which translates to higher tensile forces and impaired adhesion strengthening and cell detachment.

Keywords

Atrial natriuretic peptide; neutrophil; adhesion; inflammation

*Address for correspondence: Scott I. Simon, Department of Biomedical Engineering, 451 E. Health Sciences Drive, GBSF, Room 3313, University of California, Davis, CA 95616, USA. Tel.: +1 530 754-5739; sisimon@ucdavis.edu.

1. Introduction

Leukocyte recruitment is a necessary step in the innate immune response to infection and inflammation and is crucial for wound healing [1]. The most common leukocyte in human circulation are polymorphonuclear leukocytes, commonly denoted neutrophils (PMN). They undergo a multi-step process of recruitment at vascular sites of infection and inflammation. Inactivated or resting PMN circulate in the blood stream and a fraction are captured by tethering through E-selectin (CD62E) and P-selectin (CD62P) upregulated on the endothelial surface, which recognize leukocyte selectin (L-selectin or CD62L) and P-selectin glycoprotein ligand-1 (PSGL-1) that are constitutively expressed on the PMN surface [1]. PMN transition from selectin mediated rolling to arrest can be activated by two distinct mechanisms: β_2-integrins are allosterically activated to a high affinity conformation through inside-out signaling following ligation of G-protein-coupled receptors (GPCR), and through outside-in signaling via membrane clustering of E-selectin ligands during cell rolling [2,3]. Both pathways lead to formation of high-affinity β_2-integrin bonding with intracellular adhesion molecule-1 (ICAM-1). Formation of clusters of such bonds then triggers a flux of calcium that catalyzes F-actin polymerization, which in turn facilitates PMN shape change to a polarized shape that orients the process of migration through the endothelium towards sites of infection and inflammation [4,5]. This inflammatory response of PMN can be deleterious under hyper-inflammatory conditions such as tissue ischemia during acute myocardial infarction, which elicits a rapid increase in circulating numbers and unchecked recruitment [6,7]. Therapeutic use of antagonists to the selectins, integrins, and super-Ig adhesion molecules upregulated on leukocytes and endothelium has shown mixed results and there are currently few antibodies or small molecules available for clinical use [8,9]. This has motivated the discovery of biological strategies for ameliorating the chronic over recruitment of PMN to inflamed endothelium [8].

The discovery of atrial natriuretic peptide (ANP) has provided evidence that the heart functions not only as a pump, but also as a secretory organ that can regulate blood pressure, fluid volume, and electrolyte balance. ANP is released by muscle cells in the atria of the heart and binds guanylyl cyclase-A (GC-A) leading to biological actions through a cGMP-dependent pathway [10]. ANP has long been established as a regulator of plasma volume by acting on renal water and sodium excretion, as well as modulating vasodilation and the distribution of plasma proteins between blood and body tissue. Recent studies indicate that ANP expression is increased in infarcted regions of the left ventricle implying its potential importance in local regulation during myocardial infarction (MI) [11]. Recombinant ANP (carperitide) was approved for treatment of acute heart failure in Japan in 1995. However, the FDA in the USA has yet to approve it for treatment and the majority of studies regarding ANP are performed in Japan in patients with decompensated heart failure [12]. One large observational study was conducted on 3777 patients with acute heart failure, in which carperitide was given at an average dosage of 85 ng/kg/min for 65 h, resulting in a clinical improvement in 82% of patients [13]. While the action of carperiptide has been attributed mainly to its renal and vasodilatory actions, ANP's effects on cell rheology and endothelial permeability have motivated studies to understand the actions of ANP in attenuation of the

inflammatory recruitment of leukocytes that are reported to reduce left ventricular remodeling following MI [14].

The role of ANP as a modulator of the innate immune response to tissue injury is not well defined in part because different mechanisms of action of ANP have been ascribed to a variety of mechanisms in a diversity of cell types involved in the innate immune response, including endothelium, PMNs, mast cells, and macrophages [15]. For example in LPS-induced acute lung injury in mice, ANP was reported to reduce E-selectin upregulation on pulmonary artery endothelial cells and the release of tumor necrosis factor-alpha (TNF-α) [16]. There are also reports of ANP acting on cytoskeletal components including regulation of the actin capping protein HSP27 that promotes conversion of G- to F-actin [17] and contraction of microtubules via Rho dependent pathways [18]. ANP has also been shown to inhibit lipopolysaccharide (LPS)-induced Nitric Oxide release in macrophages by binding to NPR-A receptors to increase cGMP [15]. An increase in cGMP can inactivate Nuclear Factor-kappa B and increase cytosolic calcium in murine macrophages [17]. The effects of ANP on PMN function following activation has been controversial, with reports of ANP acting to prime PMN for activation but also to attenuate release of super oxide and matrix metalloproteins [16,19–21].

ANP primarily induces its biological effects through natriuretic peptide receptors (NPR) A and C. NPR-A activates particulate guanylate cyclase thereby increasing guanosine 3′, 5′-cyclic monophosphate (cGMP) while NPR-C regulates adenylate cyclase and membrane/lipid turnover by activation of specific phospholipases. Both Human macrophages and THP-1 cells reportedly express natriuretic peptide receptors (NPR-A, -B, and -C) [22]. Further, macrophages treated with ANP enhance reactive oxygen species (ROS) production primarily via natriuretic peptide receptor-C (NPR-C). In the case of endothelium, ANP's affects are largely attributed to NPR-A, which is densely expressed in the microvasculature. ANP is reported to increase vascular permeability under some conditions and to protect the vascular barrier to leakage under others by affecting endothelial cAMP levels via endothelial cell phosphodiesterases 2A and 3A and the levels of cGMP [23].

The goal of the current study is to delve into the actions of ANP on PMN activation and recruitment to inflamed endothelium. We report that ANP reduces PMN rolling, arrest, and transendothlial migration through a mechanism independent of alterations in expression and function of adhesion receptors on the endothelium and PMN. Cell rolling and the transition to arrest is modulated by bulk cell deformation, microvillus deformability, and receptor–ligand binding kinetics [24–26]. A remarkable observation is that capture of PMN via selectins, which mediates tether formation and rolling, converted to shear resistant integrin dependent arrest with lower efficiency in the presence of ANP. This was due to abrupt rupture of long tethers that formed as shear was incrementally ramped. Rheological analysis of PMN deformation using micropipette aspiration revealed that ANP enhances PMN viscosity and this correlated in a dose dependent manner with diminished recruitment efficiency on inflamed vasculature.

2. Methods

2.1. Antibodies, small molecules, and other reagents

Recombinant human ICAM-1-Fc, E-selectin-Fc, and CXCL8/IL-8 were purchased from R&D Systems (Minneapolis, MN; Catalog No. 720-IC, 724-ES, and 208-IL respectively). Protein A/G was purchased from Fischer Scientific (Pittsburgh, PA). BS3 crosslinker, Alexa Fluor 488 Phalloidin and Vybrant DiI Cell-Labeling solution was purchased from life technologies (Grand Island, NY). Antibodies used in flow cytometry, FITC mouse anti-human CD106 (VCAM-1), PE-Cy5 mouse anti-human CD62E (E-selectin), and PE-Cy5 mouse anti-human CD54 (ICAM-1) were purchased from BD Biosciences (San Jose, CA) while Alexa Fluor 488 mouse anti-human CD11a/CD18 (mAb24, LFA-1), PE mouse anti-human CD162 (PSGL-1), and PE-Cy5 mouse anti-human CD62L (L-selectin) were purchased from Biolegend (San Diego, CA). Antibodies were used at a saturating concentration of 5 μg/ml or per manufacturer's instruction. Human atrial natriuretic peptide (ANP) was purchased from BACHEM (Torrance, CA). Normal human primary umbilical vein endothelial cells (HUVEC) were purchased from ATCC (Manassas, VA). Recombinant human IL-1β was purchased from eBioscience (San Diego, CA).

2.2. Wound model in Lys-M-EGFP mice

The Lys-M-enhanced green fluorescent protein (EGFP) stable mouse strain and the skin wound model for non-invasive whole animal fluorescent imaging of EGFP neutrophils was performed as previously described [27]. In brief, mice were anesthetized and hair was removed with a mechanical shaver prior to a 6 mm in diameter full thickness wound was made using a biopsy punch (Robbins Instruments, Chatham, NJ). The *in vivo* imaging of EGFP neutrophils appearing on the flank of mice with skin wounds was performed using whole animal fluorescence imaging system (Xenogen IVIS 100 system, Xenogen) as the neutrophils were visualized using a GFP filter (excitation 445–490 nm and emission 515–575 nm). We have previously measured the steady accumulation of EGFP labeled PMNs in the wound for an hour, 24 h post wounding [27]. The rate of accumulation of PMN 24 h post wounding was stimulated over a period of 1 h after adding thrombin (5 U/ml, Sigma-Aldrich) to the wound. Direct perfusion of 50 ng/kg BW/min of ANP and its effect on the rate of accumulation of PMNs (arbitrary fluorescence intensity/min, FI/min) was measured, as previously described [27].

2.3. Neutrophil isolation

PMNs were isolated from freshly collected human blood from healthy donors consented through an approved by the University of California, Davis institutional review board protocol. Whole blood was layered over PMN separation media, Polymophoprep purchased from Axis Shield formulations purchased from Cosmo Bio USA, as previously described [1]. After centrifugation PMN cells were extracted and washed with 4-(2-hydroxyethyl)-1-piperazineethanesulfonic acid buffered salt solution. PMN were treated with ANP (0–100 nM) for 30 min at room temperature under agitation prior to use.

2.4. Flow cytometry

Flow cytometry was used to quantify the presence of VCAM-1, ICAM-1, and E-selectin on HUVEC in the presence and absence of ANP. HUVEC monolayers were grown to high confluence overnight according to ATCC supplied protocols. HUVEC monolayers were then treated with 0.2 ng/ml of IL-1β for 4 h and incubated with ANP (0–100 nM) 30 min prior to harvesting. Cells were harvested via 1 mM EDTA chelation and spun down. After collection, suspended cells were incubated with FITC conjugated mouse anti-human CD54 and PE-Cy5 conjugated mouse anti-human CD62E or PE-Cy5 conjugated mouse anti-human ICAM-1. Flow cytometry was also used to quantify ANPs ability to activate PMNs in suspension and alter actin polymerization. Whole blood was obtained by venipuncture and PMNs were immediately isolated and treated with ANP (0–10 nM) for 30 min. Cells were then incubated with Alexa Fluor 488 mouse anti-human mAb24 to label high affinity LFA-1, PE mouse anti-human PSGL-1, and PE-Cy5 mouse anti-human L-selectin, or Alexa Fluor conjugated Phalloidin with simultaneous fixing and permeabilization, with and without IL-8 stimulation. Data was acquired by flow cytometry (BD FACScan) and quantified (FlowJo) as mean fluorescent intensity and plotted as fold change compared to 0 nM ANP conditions. All experiments were performed in triplicates.

2.5. Adhesion assays

HUVECs were cultured onto 35 mm diameter, #1.5 glass coverslips over to tight confluence as per supplied ATCC protocols. HUVEC monolayers were then treated with 0.2 ng/ml of IL-1β for 4 h and incubated with ANP (0–100 nM) 30 min prior to use. Custom multi-channel microfluidic device were assembled on coverslips as previously described [2,4,5] and isolated PMNs were perfused at a concentration of 1×10^6 cells/ml at a physiological shear of 2 dynes/cm^2. For adhesion strengthening experiments 25 mm diameter, #1.5 glass coverslips were piranha etched to remove organic molecules and to deposit hydroxyl group molecules on the surface. The etched coverslips were submerged in Acetone with 1% 3-aminopropyltriethoxysilane (APTES) to add aminosilane groups and recombinant human ICAM-1-Fc along with E-selectin-Fc were absorbed at 5 μg/ml concentration for 1 h, resulting in approximately 2000 sites/μm^2. Isolated human PMNs at 10^6 cells/ml treated with ANP (0–100 nM) were allowed to settle over the ICAM-1 + E-selectin substrate. Shear was then ramped at 30 s intervals from 0, 4, 10, 20, to 40 dynes/cm^2, and the number of cells that remained adhered were measured over seven separate fields of view along the centerline of the channel at each shear level. Cell arrest was defined as a PMN that translated on the substrate less than 50% of a cell diameter (~4 μm) in a 10 s interval.

2.6. Rheological analyses

Micropipettes with an evenly broken, cylindrical tip of the desired inner diameter (~2 μm for hemisphere aspiration and ~4 μm for full aspirations) were made prior to experimentation, as described previously [2]. To ensure PMN quiescence while imaging 10% heat treated autologous serum was added to the experimental buffer and coated the chamber and micropippettes. A small volume of cell suspension at 1×10^6 cells/ml was introduced into the experimental chamber (~5 μl). Assuming cortical tension, γ, is uniform and isotropic

Laplace's law can be used in terms of aspiration pressure within the pipette to solve for cortical tension, σ.

$$\sigma=\frac{1}{2}\frac{\Delta pRR_p}{R-R_p},$$

where R is the radius of the spherical main cell body and R_p is the pipette radius [26]. The protrusion length at every pressure and radius of the cell is estimated assuming the volume of the cell is kept constant. The radius of the outer portion of the cell was calculated by the following geometrical equation:

$$R=\left(R_i^3-\frac{3}{4}R_p^2L_p+\frac{1}{4}R_p^3\right)^{1/3},$$

where R_i is the radius of the untouched cell and R_p is the radius of the pipette. Cell surface area was then estimated by describing cell geometry in terms of spherical and cylindrical components and tension was then computed using Laplace's equation. The cortical tension is obtained by plotting the fractional increase in area expansion from 0 to 0.35 as PMN are aspirated to different extents. Resting cortical tension was inferred from the data by fitting a straight line to the low-pressure values and the *y*-intercept of the linear fit is a measure of the resting cortical tension. To estimate the elastic constants of PMN recovery a derivative of the classical "cortical shell-liquid core model" was implemented. The analysis provides an approximate analytical solution to the equations of creeping flow of a Newtonian droplet with a moving, pre-stressed boundary [28–31]. The model assumes a constant cortical tension and predicts the time dependent recovery, measured as the ratio of cell length to width. Custom-written software interfaced with a joystick allowed for three dimensional manipulation of the micropipettes in three dimensions and video was recorded (30 frames per s) of the gentle aspiration of cells. For the full aspiration experiments cells are slowly pulled entirely into the pipette and held there for 10 s prior to being ejected back into the chamber. A Tran-Son-Tay model was used to study the time dependence of the ratio of length/width of the recovering PMN resulting in an estimate of the ratio between cortical tension and viscosity, σ/η [28,29].

2.7. Quantitative dynamic footprinting

An inverted TIRF research microscope (Nikon) equipped with a 60× numerical aperture 1.5 immersion TIRF objective and a motorized stage using a 543 solid state lasers as TIRF excitation light sources and the appropriate filter set. A 120 W arc lamp was used to capture epi-fluorescence images. Images were captured using a 16-bit digital complementary metal oxide semiconductor (CMOS) camera (Andor ZYLA) connected to a PC (Dell) with NIS Elements imaging software. Images were captured with 2 × 2 binning at a resolution of 1024 × 1024 at a rate of 2 frames per s. An incidence angle of approximately $\theta = 70°$ was used for all quantitative dynamic footprinting (qDF) experiments. Isolated PMNS at 1×10^6 cells/ml were stained with Vybrant membrane dye DiO and flown in to our custom microfluidic chip at 1 dyne/cm^2 along with high affinity LFA-1 antibody mAb24 slowly and allowed to adhere

on an ICAM-1 + E-selectin substrate. Shear was ramped incrementally from 2 to 20 dynes/cm^2 and cell contact area was observed along with focal adhesion complexes of LFA-1.

2.8. Data analysis and statistics

Data are reported as mean ± SEM. Multiple groups were compared using one-way ANOVA with Tukey posttest. All analyses were carried out using GraphPad Prism 5.01 for Windows (GraphPd Software, San Diego, CA).

3. Results

3.1. ANP down-regulates PMN recruitment on inflamed endothelium independent of changes cell adhesion molecule function

In a full thickness skin wound on the flank of a mouse, we measured the steady accumulation of LysM-EGFP labeled PMN into the wound bed 24 h following injury using whole animal fluorescence imaging (Fig. 1(A)) [27]. ANP (50 ng/kg BW/min) perfused directly into the wound bed for 60 min. elicited a small but not significant reduction compared to the baseline number of PMN accumulating in the wound. The addition of thrombin directly to the wound increased the rate of PMN influx by ~5-fold. Pretreatment with ANP for 30 min. significantly reduced the PMN influx in response to thrombin stimulation. Given that ANP in the circulation has a half-life of ~15 min [32], the average ANP concentration in the wound was estimated to be 50–75 nM. Under identical experimental conditions, a separate study by our group revealed that ANP actually increased the vascular permeability of fluorescently labeled albumin into the wound bed [33]. On the basis of these observations we investigated the mechanism by which ANP could modulate PMN interaction with endothelium over a range of ANP concentrations employing an *in vitro* model. HUVEC monolayers were inflamed with IL-1β in the presence of ANP to observe its capacity to alter the normal up-regulation of cellular adhesion molecules ICAM-1, VCAM-1, and E-selectin (Fig. 1(C)). Expression of cellular adhesion molecules was quantified using fluorescently conjugated antibodies and detected by flow cytometry on fixed and labeled HUVEC. A 300-fold increase in E-selectin, a 20-fold increase in ICAM-1, and a 3-fold increase in VCAM-1 were measured in response to inflammatory stimulation. No significant effect on the upregulation of the adhesion molecules was observed over a physiological dose range of ANP after IL-1β induced upregulation. Thus, ANP effectively decreased PMN recruitment to inflamed endothelium independent of any affect on up-regulated endothelial cell adhesion receptors.

To further understand how ANP may inhibit PMN accumulation, isolated PMNs were pretreated with ANP and perfused over HUVEC monolayers and observed using phase contrast light microscopy in a custom microfluidic flow channel [2,4,5]. PMN were sheared at 2 dynes/cm^2 in order to quantify the multistep process of cell capture and the transition from rolling to arrest. Upon arrest, PMN undergo a rapid shape change defined as ~50% of cell area converting to phase dark appearance. The frequency of PMN rolling and arrest at a low shear stress of 2 dynes/cm^2 was significantly reduced by ~50% at 10 and 100 nM ANP compared to controls ($p < 0.01$) following pretreatment (Fig. 2(A)). Of the PMN that

achieved firm arrest, ~75% underwent shape change and transendothelial migration (TEM), which was not inhibited by ANP treatment (Fig. 2(A)).

To elucidate ANP's effect on PMN adhesion strengthening following cell arrest independent of its effect on the endothelium, PMN were perfused through the microfluidic flow channel on a substrate of recombinant E-selectin and ICAM-1. This combination of endothelial adhesion receptors supports E-selectin mediated slow rolling and CD18 activation and shear resistant arrest [3,4]. To further examine the dose dependent action of ANP, shear was incrementally ramped from 2 to 40 dynes/cm^2 and the fraction of PMN remaining attached to the substrate was measured (Fig. 2(B)). PMN treated with ANP demonstrated a significantly diminished capacity to convert to shear resistant arrest. Control PMN formed short tethers upon conversion to an arrested state, those treated with ANP consistently formed long tethers that abruptly ruptured causing PMN to return to the flow field. A dose dependence was detected in which half the PMN detached at a shear stress of 20–30 dynes/cm^2 at 1 nM ANP. At the higher dose of 10 nM ANP, detachment of half the PMN was observed at 10–20 dynes/cm^2. At the high dose of ANP, complete detachment was observed at 30 dynes/cm^2. During shear ramping from 2 dynes/cm^2 to 10 dynes/cm^2, the dynamics of tether formation was recorded for firmly adherent PMN as shear was ramped from 2 dynes/cm^2 to 10 dynes/cm^2. To quantify deformation of PMN sheared in the flow channel, the maximum tether length is plotted as a function of the dose of ANP. This reveals a significant increase in tether length prior to detachment compared with untreated control (Fig. 2(C)). Taken together, the adhesion behavior of PMN indicates that cell activation and changes in rheology may be affected by treatment with ANP.

To evaluate the effect of ANP on the signaling of PMN activation in response to stimulation with IL-8, conversion of CD18 to high affinity was detected using the activation reporter antibody mAb24 and shedding of L-selectin was quantified as a loss of antibody binding (Fig. 2(D)). In response to stimulation, PMN registered a 10 fold upregulation in the high affinity state of β_2-integrin and shed L-selectin to levels equivalent to binding of IgG control antibody. The presence of ANP at 1 or 10 nM had no effect on these measures of PMN activation compared to untreated conditions. To determine if ANP altered cytoskeletal activation total F-actin expression was measured with Phalloidin in PMN stimulated with IL-8 in suspension (Fig. 2(D)). No significant change in these measures of PMN activation were observed between PMN stimulated in presence of vehicle control versus ANP treatments.

3.2. ANP increases PMN viscosity without changing cortical tension

To quantify the viscoelastic properties of PMN the ratio between cortical tension (σ) and viscosity (η) was examined by direct manipulation in micropipette studies. Cell relaxation from a deformed cylinder back to a spherical state following aspiration into a micropipette and release, was measured in isolated unstimulated PMN. Cells were subjected to deformation and held in the micropipette for 10 s and then gently expelled into the chamber (Fig. 3(A)). Cell recovery back to a spherical shape as a function of time required ~70 s for untreated cells and ~120 s in the presence of 10 nM ANP. An estimate of the ratio between cortical tension and viscosity (σ/η) is given as a fitting parameter in the "cortical shell-liquid

core" model of cellular mechanics (see Methods) as depicted by the histograms that compares untreated with 10 nM ANP treated (Fig. 3(C)). ANP resulted in a 40% decrease in the ratio of cortical tension/viscosity ($\sigma/\eta_{\text{untreated}} = 0.117$ and $\sigma/\eta_{\text{ANP}} = 0.070$).

Next we measured resting cortical tension by partially aspirating PMN at defined micropipette pressure and measured the projection length (L_p) as pressure was increased in until the projection length remained constant (Fig. 3(D)). Using the analysis described in methods resting cortical tension was found to be 0.021 ± 0.003 nN/m for untreated cells and 0.023 ± 0.007 nM/m for 10 nM ANP treatments. No significant difference in the magnitude of the resting cortical tension was found between controls versus ANP treatment. Measured values of σ and σ/η in PMNs were not significantly different from previous reports of human granulocytes (Table 1). Our value of cytoplasmic viscosity for untreated cells was ~179 Pa · s, which is in close agreement with previous observations (25–28, 32–34), whereas those treated with ANP were nearly 1-fold higher at a value of ~324 Pa · s. We conclude that ANP elicited a significant increase in cytosolic viscosity even in the absence of PMN activation.

3.3. ANP decreases PMN deformability and adhesive footprint on ICAM-1 under shear flow

PMN were labeled with the membrane dye Vybrant DiO and sheared in microfluidic channels on an E-selectin and ICAM-1 substrate at a shear stress of 1 dynes/cm^2 to promote cell rolling and arrest. Shear was then incremented and the change in membrane contact area of adhesive PMN was determined over time using TIRF microscopy. As depicted in the fluorescence images, PMN establish an initial area of contact and steadily become elongated in the direction of shear flow (Fig. 4(A)). PMN formed a smaller area of contact in the presence of ANP and did not exhibit an increase in area over time at constant shear stress (Fig. 4(B)). As shear stress was incremented, untreated PMN nearly tripled the area of adhesive contact, while for ANP treated cells the area remained constant (Fig. 4(C)). Since it was observed that exposure to 10 nM ANP elicited premature detachment in the majority of PMN as shear was ramped to 10 dynes/cm^2, we examined the formation of high affinity CD18 bonds to ICAM-1 in untreated and ANP treated adherent PMN (Fig. 4(D)). Consistent with expression of high affinity CD18 in stimulated suspensions of PMN, the overall level of CD18 in contact with ICAM-1 following rolling to arrest was equivalent for untreated and ANP treated PMN. However, formation of focal clusters of CD18 bonds was significantly diminished in presence of ANP as compared with untreated PMN. Formation of high affinity CD18 bond clusters is required for PMN adhesion strengthening following arrest and spreading on the substrate [34]. We conclude that ANP treatment disrupts the capacity of attached PMN to deform and spread on the substrate resulting in a smaller adhesive footprint containing fewer CD18 bond clusters that prematurely fail compared with normal adhesion strengthening.

4. Discussion

ANP is produced by the heart during atrial distension and has been shown to be a modulator of the innate immune response, yet detailed studies of ANP's anti-inflammatory mechanisms relevant to reduction of PMN interaction with the endothelial wall have not

been investigated [15,36,37]. ANP has previously been used to treat patients with heart failure due to its diuretic and vasodilatory actions [13,14]. However, anti-inflammatory effects, especially to reduced PMN interaction with activated endothelium, have not been investigated. Directly imaging PMN trafficking into a full thickness skin wound, we observed acute treatment with ANP exerted a significant inhibitory effect on thrombin stimulated PMN recruitment. Thrombin activates Proteinase-activated receptors (PAR) 1 and 4 to induce a proinflammatory phenotype through upregulation of VCAM-1, ICAM-1, and E-selectian [38,39]. Thrombin stimulated adhesion is different from chemokine stimulated adhesion (such as fMLP and IL-8) signaling that occurs primarily in PMN. A classical signaling pathway triggered by GPCR is the biphasic Calcium-signal. The first phase of which is mediated by phospholipase Cβ that leads to generation of IP_3 and release of calcium from intracellular stores. Activation of phosphatidylinositol P_3 (PIP_3) has also been implicated in GPCR stimulation via Src-Family kinases. The TNF-receptor family can also signal PMN activation and prime subsequent response to additional stimuli by recruiting adaptor proteins (TNFR1 and TNFR2, both present on PMN) [40]. We assessed the mechanism using an *in vitro* assay in which PMN were sheared over HUVEC and discovered that ANP down-regulated their recruitment to inflamed endothelium by ~40% primarily though antagonizing the transition to shear resistant integrin-ICAM-1 mediated arrest. It is noteworthy that diminished recruitment occurred irrespective from changes in adhesion molecule expression and function on HUVEC. Measurement of PMN rheology revealed that treatment with ANP resulted in an increase in PMN cytoplasmic viscosity within minutes, while the subsurface membrane cortical tension remained constant. Single cell image analysis of adherent PMN deforming under shear stress revealed an increase in adhesive contact area and the formation of membrane tethers, which was altered by ANP treatment. We conclude that ANP effectively limits PMN recruitment to sites of inflammation by altering the normal response characterized by an increase in the area of adhesive contact as cells spread and polarize on the substrate. ANP nearly doubled PMN cytoplasmic viscosity and this corresponded to significantly smaller adhesive contact and diminished formation of durable integrin bond clusters. These observations correlated with a dose dependent increase in PMN detachment at relatively low levels of shear stress.

Previous studies on the relationship between wall shear stress and leukocyte deformation during rolling and arrest have shown that rolling velocity and frequency of arrest is invariant as shear stress is incremented. This is due to the greater deformation of PMN that occurs as hydrodynamic drag force is increased, which translates to increased contact area as depicted in the schematic of Fig. 5. As PMN spread there is more efficient conversion to cell arrest due to an increase in integrin bond formation [41]. Over the duration of rolling to arrest, PMN transition from an initially spherical state to a more flattened and elongated geometry that is attributed to its viscoelastic properties [42]. An estimate of the extent of deformation can be gleaned from application of a continuum model based upon measured material properties of the PMN under resting and activated conditions [43,44]. Dembo et al. derived a so called “tape-peeling” model to examine the dynamics of the area of adhesive contact. This model proposed the cell be divided into three regions; the macroscopic region where hydrodynamic shear forces predominate, the microscopic region where receptor–ligand binding is initiated and receptor density is low, and the adhesion layer where receptor

density increases and bond formation occurs (Fig. 5). During cell rolling to arrest, shear forces are transmitted from the cell body to the substrate through membrane tension and cell body forces. Cell deformation is critical in resisting the hydrodynamic drag that acts on rolling PMN. For example, the magnitude of shear forces acting on PMN positively correlates with the ratio of the height of the cell to vessel diameter [45]. A concomitant effect of cell deformation and membrane spreading is a decrease in the angle (θ_b) at which the resultant drag force acts on the bonds. An increase in adhesion contact area is associated with increased bond formation, effectively countering the resultant shear force (F_s) that acts to rupture nascent bonds (F_b) (Fig. 5) [46,47]. The increase in cell viscosity induced by ANP treatment was found to decrease the extent of deformation of PMN arrested on the substrate, thus resulting in a smaller contact area at constant cell volume. This decrease in cell deformation effectively reduced PMN capture, as well as their capacity to remain adherent (e.g. adhesion strengthen) with increased shear stress. We hypothesize that ANP treated PMN exhibit increased cytosolic viscosity and consequently do not flatten as much as untreated. This resulted in a greater (θ_b) and higher tensile forces acting on membrane tethers and on integrin bond clusters that form within smaller areas of adhesive contact. Tethers in ANP treated PMN were twice as long and disruptive shear forces were distributed to fewer CD18 bond clusters resulting in premature rupture at lower F_s compared with untreated cells.

The mechanism by which ANP increases PMN viscosity remains unknown and will require additional inquiry. A potential molecular mechanism by which ANP increases the cytoplasmic viscosity of PMN may act through a previously reported effector pathway for thrombin attenuation and microtubule stabilization in endothelial cells [18]. According to Baldini et al. macrophages express natriuretic peptide receptors NPR-A, NPR-B, and NPR-C and ANP treatment significantly decreases intracellular pH enhancing ROS production. Although it is possible that ANP acts via these membrane receptors in PMN, the signaling pathway has yet to be reported. ANP signaling through Rac GTPase and its effector PAK1, which down-regulates GEF-H1 activation via phosphorylation at Ser^{855}. One downstream consequence is reduced activation of Rho-GTPases, which are key regulators of actin dynamics in vascular cells [48]. Additionally ANP has been shown to stabilize microtubules, leading to its vasoprotective effects [18]. Rac2 is another GTPase that plays a key role in PMN responses to inflammatory signaling, including actin remodeling, chemotaxis, and superoxide production by NADPH oxidase [49,50]. Given the observation that the cellular level of F-actin was not different between ANP and untreated PMN, we hypothesize that ANP may alter the dynamic localization of F-actin, possibly by influencing gelsolin dynamics through stimulation of Rac-GTPase [50,51]. It has been shown that blocking F-actin formation with Cytochalasin B inhibits tether formation of PMN rolling in shear flow to E- and P-selectin (e.g. reduces microvilli numbers in cells). This was observed to increase the strength of rolling adhesions on E- and P-selectin and increased substrate contact due to cell deformability [52]. Rac has been shown to promote the dissociation of gelsolin from actin filaments in neutrophils thereby effecting F-to G-actin ratio [53]. Thus, we speculate that ANP may disrupt the normal process by which gelsolin regulates spatiotemporal actin dynamics and in turn affect cytosolic viscosity. This is consistent with the finding of inefficient extravasation into the full thickness skin wound in presence of ANP and the

defect in conversion to shear resistant firm arrest and adhesion strengthening. Further analysis of ANP's effect on PMN Rho-GTPases and local F-actin dynamics is necessary to further elucidate its apparent effect on PMN viscosity.

In this study, we report that ANP significantly attenuates the thrombin augmented inflammatory accumulation of PMN in skin wounds. We attribute this to ANP capacity to increase cytosolic viscosity and provide a potential mechanism to explain the observation of diminished PMN deformation and an inability to convert to shear resistant arrest. Further studies on the relation between ANP and spatiotemporal control of F-actin dynamics and in turn the effect on PMN viscosity could lead to its use as anti-inflammatory inside and outside of Japan.

References

1. Simon SI, Green CE. Molecular mechanics and dynamics of leukocyte recruitment during inflammation. Annu Rev Biomed Eng. 2005; 7:151–85. [PubMed: 16004569]
2. Dixit N, Kim MH, Rossaint J, Yamayoshi I, Zarbock A, Simon SI. Leukocyte function antigen-1, kindlin-3 and calcium flux orchestrate neutrophil recruitment during inflammation. J Immunol. 2012; 189:5954–64. [PubMed: 23144497]
3. Abram CL, Lowell CA. The ins and outs of leukocyte integrin signaling. Annu Rev Immunol. 2009; 27:339–62. [PubMed: 19302044]
4. Dixit N, Yamayoshi I, Nazarian A, Simon SI. Migrational guidance of neutrophils is mechanotransduced via high-affinity LFA-1 and calcium flux. J Immunol. 2011; 187:472–81. [PubMed: 21632714]
5. Schaff UY, Dixit N, Procyk E, Yamayoshi I, Tse T, Simon SI. Orai1 regulates intracellular calcium, arrest, and shape polarization during neutrophil recruitment in shear flow. Blood. 2010; 115:657–66. [PubMed: 19965684]
6. Haumer M, Amighi J, Exner M, Mlekusch W, Sabeti S, Schlager O, et al. Association of neutrophils and future cardiovascular events in patients with peripheral artery disease. J Vasc Surg. 2005; 41(4): 610–7. [PubMed: 15874924]
7. Amulic B, Cazalet C, Hayes GL, Metzler KD, Zychlinsky A. Neutrophil function: From mechanisms to disease. Annu Rev Immunol. 2012; 30:459–89. [PubMed: 22224774]
8. Chase SD, Magnani JL, Simon SI. E-selectin ligands as mechanosensitive receptors on neutrophils in health and disease. Ann Biomed Eng. 2012; 40(4):849–59. [PubMed: 22271244]
9. Mitroulis I, Alexaki VI, Kourtzelis I, Ziogas A, Hajishengallis G, Chavakis T. Leukocyte integrins: Role in leukocyte recruitment and as therapeutic targets in inflammatory disease. Pharmacol Ther. 2015; 147:123–35. [PubMed: 25448040]
10. Saito Y. Roles of atrial natriuretic peptide and its therapeutic use. J Cardiol. 2010; 56:262–70. [PubMed: 20884176]
11. Mizuno Y, Yasue H, Oshima S, Yoshimura M, Ogawa H, Morita E, et al. Effects of angiotensin-converting enzyme inhibitor on plasma B-type natriuretic peptide levels in patients with acute myocardial infarction. J Card Fail. 1997; 3:287–93. [PubMed: 9547443]
12. Biselli R, Farrace S, De Simone C, Fattorossi A. Potentiation of human polymorphonuclear leukocyte activation by atrial natriuretic peptide. Inhibitory effect of carnitine congeners. Inflammation. 1996; 20:33–42. [PubMed: 8926047]
13. Suwa M, Seino Y, Nomachi Y, Matsuki S, Funahashi K. Multicenter prospective investigation on efficacy and safety of carperitide for acute heart failure in the 'real world' of therapy. Circ J. 2005; 69(3):283–90. [PubMed: 15731532]
14. Hayashi M, Tsutamoto T, Wada A, Maeda K, Mabuchi N, Tsutsui T, et al. Intravenous atrial natriuretic peptide prevents left ventricular remodeling in patients with first anterior acute myocardial infarction. J Am Coll Cardiol. 2001; 37(7):1820–6. [PubMed: 11401117]

15. Vollmar AM. The role of atrial natriuretic peptide in the immune system. Peptides. 2005; 26(6): 1086–94. [PubMed: 15911076]
16. Nojiri T, Hosoda H, Tokudome T, Miura K, Ishikane S, Okumura M, et al. Atrial natriuretic peptide prevents cancer metastasis through vascular endothelial cells. Proc Natl Acad Sci USA. 2015; 112(13):4086–91. [PubMed: 25775533]
17. Kiemer AK, Weber NC, Fürst R, Bildner N, Kulhanek-Heinze S, Vollmar AM. Inhibition of p38 MAPK activation via induction of MKP-1: Atrial natriuretic peptide reduces TNF-alpha-induced actin polymerization and endothelial permeability. Circ Res. 2002; 90(8):874–81. [PubMed: 11988488]
18. Tian X, Tian Y, Gawlak G, Sarich N, Wu T, Birukova AA. Control of vascular permeability by atrial natriuretic peptide via a GEF-H1-dependent mechanism. J Biol Chem. 2014; 289(8):5168–83. [PubMed: 24352660]
19. Mtairag el M, Houard X, Rais S, Pasquier C, Oudghiri M, Jacob MP, et al. Pharmacological potentiation of natriuretic peptide limits polymorphonuclear neutrophil-vascular cell interactions. Arterioscler Thromb Vasc Biol. 2002; 22(11):1824–31. [PubMed: 12426211]
20. Kiemer AK, Vollmar AM. Autocrine regulation of inducible nitric oxide synthase in macrophages by atrial natriuretic peptide. J Biol Chem. 1998; 273:13444–51. [PubMed: 9593677]
21. De Vito P. Atrial natriuretic peptide: An old hormone or a new cytokine. Peptides. 2014; 58:108–16. [PubMed: 24973596]
22. Baldini PM, De Vito P, Martino A, Fraziano M, Grimaldi C, Luly P, et al. Differential sensitivity of human monocytes and macrophages to ANP: A role of intracellular pH and reactive oxygen species production through the phospholipase involvement. J Leukoc Biol. 2003; 73(4):502–10. [PubMed: 12660225]
23. Kuhn M. Endothelial actions of atrial and B-type natriuretic peptides. Br J Pharmacol. 2012; 166(2):522–31. [PubMed: 22220582]
24. Damiano ER, Westheider J, Tözeren A, Ley K. Variation in the velocity, deformation, and adhesion energy density of leukocytes rolling within venules. Circ Res. 1996; 79:1122–30. [PubMed: 8943950]
25. Firrell JC, Lipowsky HH. Leukocyte margination and deformation in mesenteric venules of rat. Am J Physiol. 1989; 256:1667–74.
26. Sundd P, Gutierrez E, Pospieszalska MK, Zhang H, Groisman A, Ley K. Quantitative dynamic footprinting microscopy reveals mechanisms of neutrophil rolling. Nat Methods. 2010; 7(10):821–4. [PubMed: 20871617]
27. Kim MH, Curry FR, Simon SI. Dynamics of neutrophil extravasation and vascular permeability are uncoupled during aseptic cutaneous wounding. Am J Physiol Cell Physiol. 2009; 296(4):C848–56. [PubMed: 19176758]
28. Tran-Son-Tay R, Needham D, Yeung A, Hochmuth RM. Time dependent recovery of passive neutrophils after the large deformation. Biophys J. 1991; 60(4):856–66. [PubMed: 1742456]
29. Tran-Son-Tay R, Kirk TF 3rd, Zhelev DV, Hochmuth RM. Numerical simulation of the flow of highly viscous drops down a tapered tube. J Biomech Eng. 1994; 116(2):172–7. [PubMed: 8078323]
30. Needham D, Hochmuth RM. Rapid flow of passive neutrophils into 4 microns pipet and measurement of cytoplasmic viscosity. J Biomech Eng. 1990; 112(3):269–76. [PubMed: 2214708]
31. Needham D, Hochmuth RM. A sensitive measure of surface stress in the resting neutrophil. Biophys J. 1992; 61(6):1664–70. [PubMed: 1617145]
32. Potter LR. Natriuretic peptide metabolism, clearance and degredation. FEBS J. 2011; 278(11): 1808–17. [PubMed: 21375692]
33. Curry FE, Jiang Y, Kim MH, Clark JF, Adamson RH, Simon SI. Atrial natriuretic peptide attenuates thrombin-induced inflammation. FASEB J. 2014; 28(1):672.4.
34. Dixit N, Kim MH, Rossaint J, Yamayoshi I, Zarbock A, Simon SI. Leukocyte function antigen-1, kindlin-3, and calcium flux orchestrate neutrophil recruitment during inflammation. J Immunol. 2012; 189(12):5954–64. [PubMed: 23144497]
35. Evans E, Yeung A. Apparent viscosity and cortical tension of blood granulocytes determined by micropipette aspiration. Biophys J. 1989; 13(9):941–54. [PubMed: 4733701]

36. Nomura F, Kurobe N, Mori Y, Hikita A, Kawai M, Suwa M, et al. Multicenter prospective investigation on efficacy, safety of carperitide as a first-line drug for acute heart failure syndrome with preserved blood pressure: COMPASS: Carperitide effects observed through monitoring dyspnea in acute decompensated heart failure study. Circ J. 2008; 72:1777–86. [PubMed: 18832779]
37. Brandt RR, Wright RS, Redfield MM, Burnett JC Jr. Atrial natriuretic peptide in heart failure. J Am Coll Cardiol. 1993; 22:86A–92A.
38. Hirano K. The roles of proteinase-activated receptors in the vascular physiologu and pathophysiology. ATVB. 2007; 27(1):27–36.
39. Vergnolle N, Derian CK, D'Andrea MR, Steinhoff M, Andrade-Gordon P. Characterization of thrombin-induced leukocyte rolling and adherence: A potential proinflammatory role for proeinase-activated receptor-4. J Immunol. 2002; 169(3):1467–73. [PubMed: 12133973]
40. Futosi K, Fodor S, Mocsai A. Reprint of neutrophil cell surface receptors and their intracellular signal transduction pathways. Int Immunopharmacol. 2013; 17(4):1185–97. [PubMed: 24263067]
41. Firrell JC, Lipowsky HH. Leukocyte margination and deformation in mesenteric venules of rat. Am J Physiol. 1989; 256:1667–74.
42. Rocheleau AD, Sumagin R, Sarelius IH, King MR. Simulation and analysis of tethering behavior of neutrophils with pseudopods. PloS ONE. 2015; 10(6):e0128378. [PubMed: 26091091]
43. Dembo M, Torney DC, Saxman K, Hammer D. The reaction-limited kinetics of membrane-to-surface adhesion and detachment. Proc R Soc Lond B Biol Sci. 1988; 234(1274):55–83. [PubMed: 2901109]
44. Ward MD, Dembo M, Hammer DA. Kinetics of cell detachment: Peeling of discrete receptor clusters. Biophys J. 1994; 67:2522–34. [PubMed: 7696491]
45. Sundd P, Pospieszalska MK, Ley K. Neutrophil rolling at high shear: Flattening, catch bond behavior, tethers and slings. Mol Immunol. 2013; 55(1):59–69. [PubMed: 23141302]
46. Liu X, Wang X, Tin H, Chen H. Deformation mechanism of leukocyte adhering to vascular surface under steady shear flow. Sci China C Life Sci. 2004; 47(2):165–74. [PubMed: 15379249]
47. Dinauer MC. Regulation of neutrophil function by Rac GTPases. Curr Opin Hematol. 2003; 10(1): 8–15. [PubMed: 12483106]
48. Lee CW, Vitriol EA, Shim S, Wise AL, Velayutham RP, Zheng JQ. Dynamic localization of G-actin during membrane protrusion in neuronal motility. Curr Biol. 2013; 23(12):1046–56. [PubMed: 23746641]
49. Arcaro A. The small GTP-binding protein Rac promotes the dissociation of gelsolin from the actin filaments in neutrophils. J Biol Chem. 1998; 273(2):805–13. [PubMed: 9422735]
50. Lõrincz ÁM, Szarvas G, Smith SM, Ligeti E. Role of Rac GTPase activating protein in regulation of NADPH oxidase in human neutrophils. Free Radic Biol Med. 2014; 68:65–71. [PubMed: 24321316]
51. Damiano ER, Westheider J, Tözeren A, Ley K. Variation in the velocity, deformation, and adhesion energy density of leukocytes rolling within venules. Circ Res. 1996; 79:1122–30. [PubMed: 8943950]
52. Finger EB, Bruehl RE, Bainton DF, Springer TA. A differential role for cell shape in neutrophil tethering and rolling on endothelial selectins under flow. J Immunol. 1996; 157(11):5085–96. [PubMed: 8943418]
53. Cao J, Donell B, Deaver DR, Lawrence MB, Dong C. In vitro side-view imaging technique and analysis of human T-leukenic cell adhesion to ICAM-1 in shear flow. Microvasc Res. 1998; 55(2): 124–37. [PubMed: 9521887]

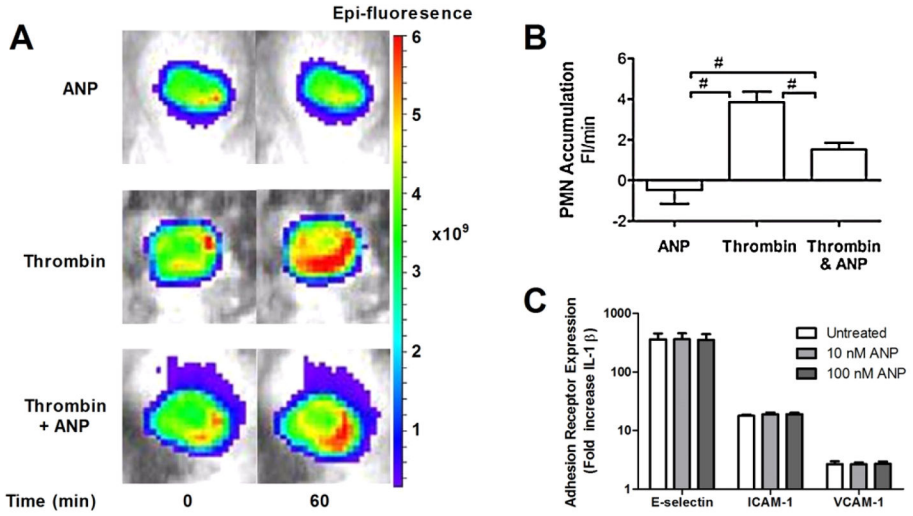

Fig. 1.

ANP down-regulates neutrophil recruitment on inflamed endothelium independent of adhesion receptor expression. (A) A full thickness skin wound was performed in Lys-M-EGFP mice and at 24 h PMN accumulation was quantified over a 60 min interval in response to Thrombin stimulation (5 U/ml) in presence and absence of perfusion of ANP (50 ng/kg/min). Representative images of PMN fluorescence intensity in the wound bed are depicted for each treatment condition. (B) PMN accumulation in wound over 60 min relative to saline control is plotted as rate of change of PMN fluorescence (Fl/min; significant attenuation versus ANP by ANOVA with Tukey multiple comparison test, $n = 6$ mice, # depicts $p < 0.05$). (C) Endothelial adhesion receptor expression was assessed on IL-1β (0.2 ng/ml) stimulated HUVEC as a function of ANP concentration. The relative increase in receptor expression normalized to the baseline level on non-stimulated endothelium is plotted ($n = 3$, mean ± SEM). No significance was found between IL-1β stimulated versus ANP. (Colors are visible in the online version of the article; http://dx.doi.org/10.3233/BIR-15067.)

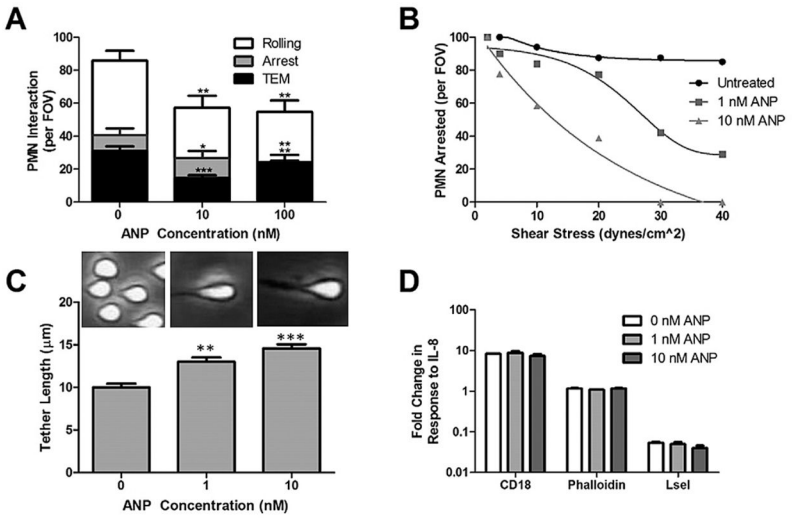

Fig. 2.

ANP inhibits PMN capture and shear resistant independent of cellular adhesion receptor activation. (A) PMN rolling, arrest, and transendothelial migration (TEM) quantified at 2 dynes/cm^2 on IL-1β inflamed HUVEC was measured from video record as mean ± SEM number per four FOVs and analyzed from 3 separate microfluidic flow channels. $n = 3$ separate donors. *** Signifies significance between ANP and vehicle control $p < 0.005$, ** signifies significance between ANP and vehicle control $p < 0.01$, and * signifies significance between ANP and control $p < 0.05$. (B) PMN (1×10^6 cells/ml) were pretreated with 1–10 nM ANP and continuously perfused over recombinant ICAM-1 + E-selectin substrates in a microfluidic flow chamber. The number of PMN remaining adherent relative to the number at 2 min under 2 dynes/cm^2. Shear was incremented every 30 s as depicted up to 40 dynes/cm^2. The numbers of PMN remaining in the presence or absence of ANP at the indicated dose were recorded from 3 separate donors. Nearly all PMN treated with vehicle control convert to shear resistant arrest, while ANP treated PMN formed long membrane tethers that abruptly ruptured upon detachment. Line plots are polynomial regression fits to the data points. (C) PMN tether formation for PMN arrested at 2 dynes/cm^2 and ramped to 10 dynes/cm^2. Images of tether length defined as point of contact with substrate to the center of the cell are shown just before cell detachment. PMN tether length significantly increased at the low and high dose of ANP treatment compared with vehicle control ($p < 0.05$, $n = 3$). (D) Isolated PMNs (1×10^6 cells/ml) were analyzed by flow cytometry for expression of β_2-integrin and L-selectin adhesion receptors following 15 min stimulation with IL-8 (10 nM) after pretreatment with the indicated dose of ANP for 30 min prior to measurement. ANP did not alter the up-regulation of β_2-integrin or the shedding of L-selectin when compared to untreated control ($n = 3$). PMN F-actin was measured using Phalloidin with and without IL-8 stimulation after simultaneous fixing and permeabilization. Data shows replicates for $n = 3$ donors with no significant effect of ANP observed.

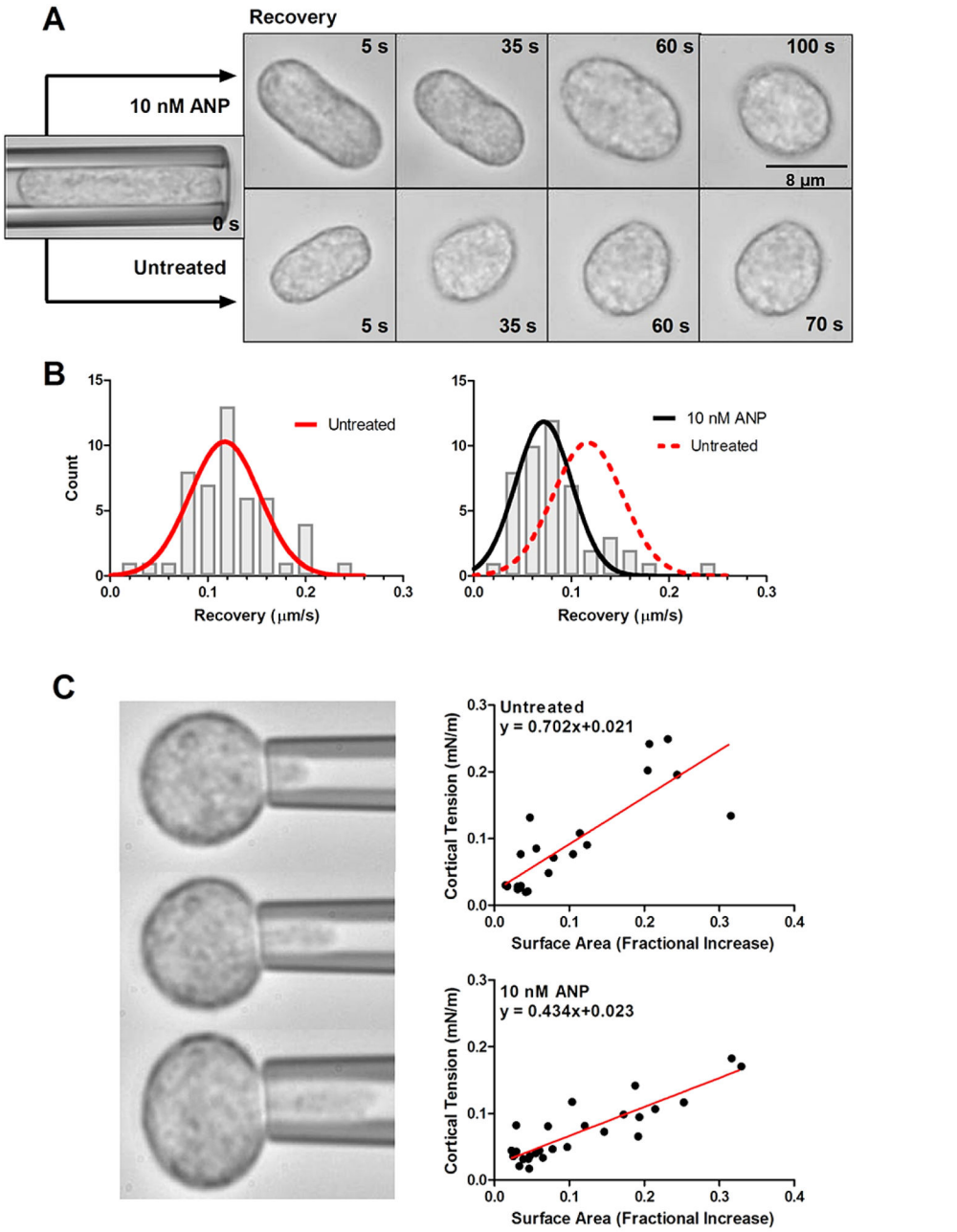

Fig. 3.

Rheological analysis of PMN cortical tension and viscosity. Untreated and 10 nM ANP treated PMN were suspended in HEPES buffered saline with 10% autologous serum to maintain unactivated and non-adherent state. (A) PMN were aspirated into the micropipette and held for 10 s prior to expulsion into the chamber. Kinetics of recovery back to spherical state (e.g. defined as length to width ratio of 1.1) was recorded and depicted in representative images. ANP treated PMN recovered ~30% slower than vehicle control. (B) Time constant for recovery was fit to a viscoelastic model yielding an estimate of cortical tension/viscosity [26,27]. Histograms of vehicle control versus ANP were Gaussian fit as depicted. Untreated PMNs (red line) versus 10 nM ANP (black) show a significant left shift in the tension/

viscosity ratio due to ANP treatment ($n = 50$ PMN per condition analyzed from $n = 4$ separate donors). (C) PMN were partially aspirated into a micropipette while internal pressure was slowly increased and plotted versus protrusion length of hemispherical cap as depicted in images. Laplace's law was used to estimate cortical tension and correlate it with a fractional increase in surface area from resting spherical state (see Methods). A linear regression was used to compute resting cortical tension in vehicle control (0.021 ± 0.013) and 10 nM ANP treated cells (0.023 ± 0.007) ($n = 50$ PMN analyzed from 4 separate experiments). No significance found between control and ANP treatment. (Colors are visible in the online version of the article; http://dx.doi.org/10.3233/BIR-15067.)

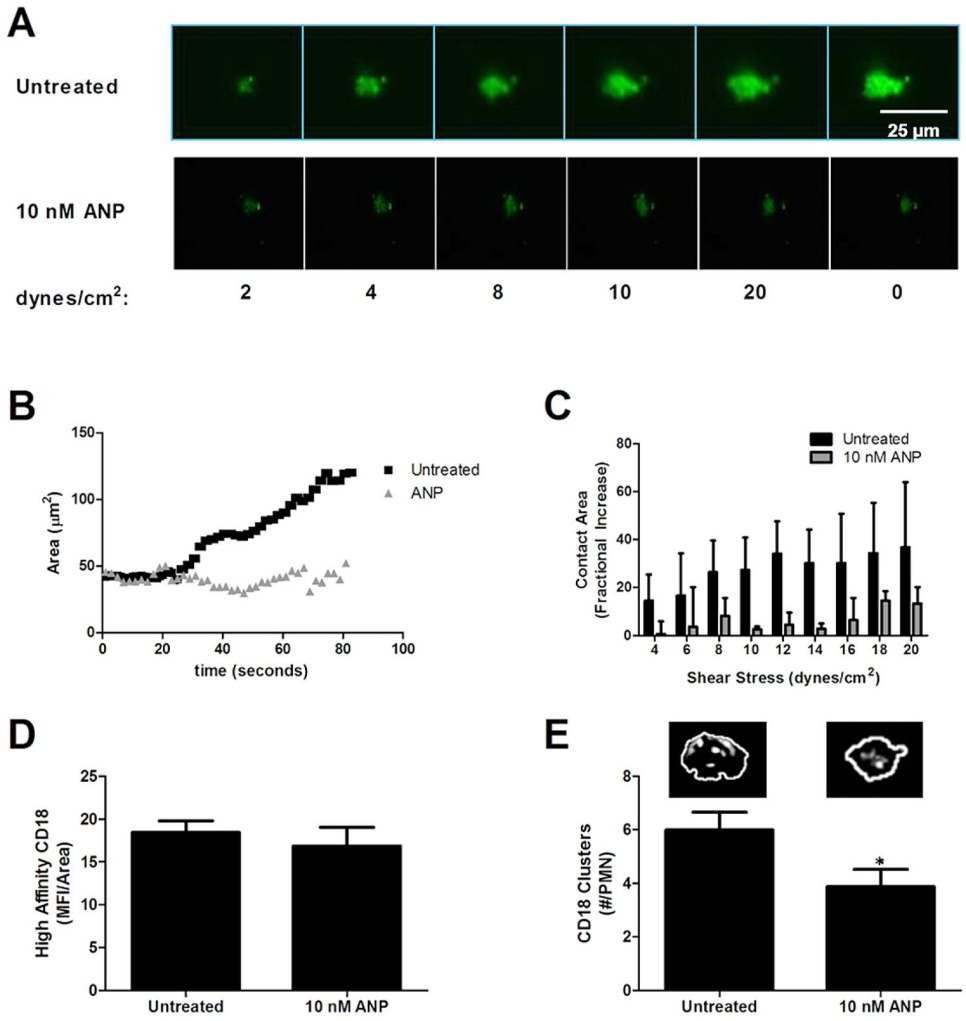

Fig. 4.

Adhesive contact area and β_2-integrin-ICAM-1 bond formation during PMN arrest and shear strengthening. Vehicle control versus 10 nM ANP treated PMN (2×10^6 cells/ml) were perfused in the microfluidic flow chamber at 1 dyne/cm^2 on a substrate of recombinant E-selectin and ICAM-1. (A) TIRF images of PMN arrested for 30 s before shear was incremented up to 20 dynes/cm^2 at which time shear stress was returned to 0 dynes/cm^2 revealing PMN remained deformed on substrate. (B) PMN membrane adhesive contact area was quantified using image analysis of the membrane dye DiO over time course of shear ramp for vehicle control versus 10 nM ANP ($n = 3$ separate donors, representative of 30 PMN per treatment). (C) Membrane contact area versus shear stress for vehicle control and ANP treatment. Fractional increase is plotted versus 2 dyne/cm^2 for 30 s for each condition, respectively ($n = 30$ PMN per condition, $n = 3$ separate donors). (D) High affinity CD18 quantified from TIRF images of mAb24-AF488 fluorescence within area of adhesive contact on PMN from previous shear ramp figure (no significance found using student t test, $n = 24$ cells over 3 donors). (E) CD18 focal adhesion clusters per PMN contact area. Representative images depict individual clusters, significance difference for the 10 nM ANP condition ($p <$

0.05, $n = 24$ cells over 3 donors). (Colors are visible in the online version of the article; http://dx.doi.org/10.3233/BIR-15067.)

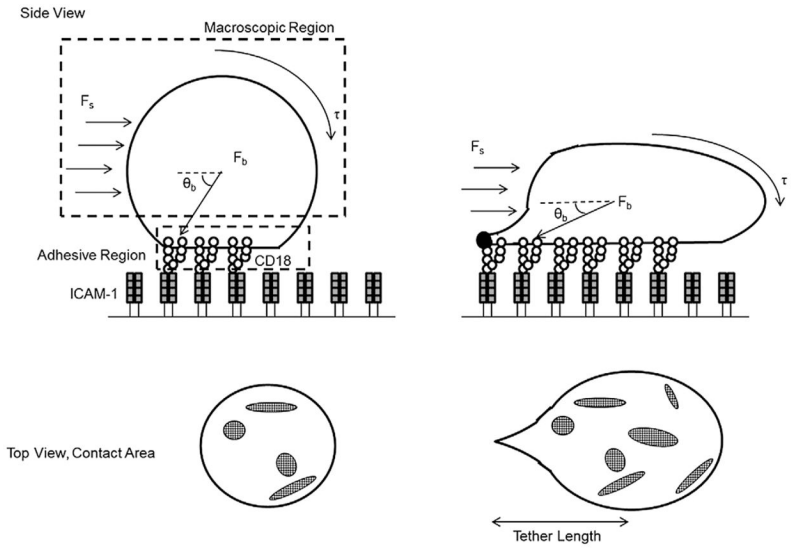

Fig. 5.

Schematic depicting PMN deformation and integrin bond formation under shear flow. PMN form stable CD18/ICAM-1 bonds that support cell arrest. The top macroscopic view depicts a PMN deforming from a spherical to a tethered and elongated geometry relative to the direction of flow (θ_b). The hydrodynamic shear force (F_s) translates membrane tension (τ) into a disruptive bond force (F_b) that act on bond clusters within the adhesive contact region. Top view depicts the increase in adhesive contact area allowing for the formation of CD18 bond clusters. With ANP treatment there is less deformation, which maintains a larger (θ_b) and greater translation of membrane tension (τ) to fewer bond clusters and thus a relative higher breakage force (F_b) on fewer bond clusters.

Table 1

Membrane tension and viscosity of PMN obtained from micropipette experiments

σ (mN/m)	σ/η (μm/s)	η (Pa · s)	Study
0.021 ± 0.013	0.117	~179	Untreated
0.023 ± 0.007	0.071	~324	10 nM ANP
0.035	N.D.	210 ± 100	[26]
N.D.	0.17	151.7 ± 39.8	[27]
0.035	0.13–0.26	N.D.	[35]
N.D.	N.D.	135 ± 54	[31]
0.024 ± 0.003	N.D.	N.D.	[32]
0.018	0.132 ± 0.043	136	[33]

Notes: A cortical shell-liquid core rheological model was applied to compute the material constants. Viscosity was approximated using the ratio of cortical tension to viscosity from the recovery/relaxation measurements and the observed cortical tension from the micropipette aspiration experiments.